J Mol Model (2010) 16:1797–1807
DOI 10.1007/s00894-010-0730-8

ORIGINAL PAPER

Structural and energetic consequences of oxidation of d(ApGpGpGpTpT) telomere repeat unit in complex with TRF1 protein

Piotr Cysewski · Przemysław Czeleń

Received: 14 December 2009 / Accepted: 21 April 2010 / Published online: 13 May 2010

Abstract The configuration hyperspace of canonical and oxidized 14-mers of B-DNA comprising telomere repeat units d(ApGpGpGpTpT) was sampled over 40 ns *via* molecular dynamic (MD) simulations. The energetic and structural consequences of TRF1 binding to telomere B-DNA were compared with non-complexed systems. Energetic properties of analyzed pairs, di- and tri-nucleotide steps occurring in central telomere repeat unit were estimated by means of advanced quantum chemistry computations including not only BSSE corrections, electron correlation contributions but also non-negligible many-body terms. These data along with bases pair and base step parameters distributions allow for quantization of consequences of oxidation and/or TRF1 binding to telomere repeat units. Occurrence of 8-oxoguanine in central telomeric triad (CTT) is the source of high stiffness if compared to non-modified oligomer. The origin of this property comes from significantly alteration of intermolecular interactions introduced by 8-oxoguanine. The increased stability observed for base–base interactions are accumulated and characterizes also di- and tri-nucleotides. The observed changes in the intermolecular interactions originate from structural alterations imposed by TRF1 binding to canonical and oxidized telomere B-DNA. First and most direct consequence of TRF1 binding to oxidized telomere repeat unit is alteration of *shift-slide* correlations if compared to canonical system. This in turn leads to large differences in purine-purine overlapping in oxidized structures. Thus, oxidized telomere B-DNA double strands are sensitive to interactions with protein ligands and numerous structural and energetic changes are imposed on base pairs forming CTT.

Keywords Many-body contributions · Nucleobases interactions · Oxidative damage · 8-oxoguanine · Stacking · Telomere · TRF1

Electronic supplementary material The online version of this article (doi:10.1007/s00894-010-0730-8) contains supplementary material, which is available to authorized users.

P. Cysewski · P. Czeleń
Physical Chemistry Department, Collegium Medicum,
Nicolaus Copernicus University,
Kurpińskiego 5,
85-950 Bydgoszcz, Poland

P. Cysewski (✉)
General Chemistry Department,
University of Technology and Life Sciences in Bydgoszcz,
Faculty of Chemical Technology and Engineering,
Seminaryjna 3,
85-326 Bydgoszcz, Poland
e-mail: piotr.cysewski@cm.umk.pl

Introduction

Telomeres are important biological complexes playing a crucial role in preserving genome stability [1]. Their main function is stabilization of chromosome ends and protecting them from being recognized as B-DNA double strand breaks [2]. In humans all telomeric B-DNA fragments consist of several kilobases of six nucleotides sequences (AGGGTT) constituting so-called telomere repeat unit (TRU) [3]. These chromosomes tails are shortened with every cell division by about 20–200 base pairs, therefore often they are called “miotic clocks” [4–6]. There are specific protein ligands called TRF1 [3] and TRF2 [7] that can attach to telomere B-DNA in cells. Both these proteins interact with telomeric AGGGTT sequences by binding to major grove *via* strong contacts of different types [8]. Among many stabilization contributions there are produced distinctive hydrogen bonds between amino acids residues

and G-C base pairs in GGG triplet [8]. Also direct interactions with ribose phosphate backbone on both sides of the major groove and N-terminal arm [9] are important. Stability of this complex is highly sensitive to mild oxidative stress-induced by hyperoxia, mitochondrial dysfunction, presence of arsenic or exposure to UV irradiation [10, 11]. Occurrence of oxidative lesions in the telomeric fragment significantly affects process of DNA-protein complexes formation. Presence of one 8-oxoguanine molecule in the central telomeric triad (CTT) reduces the affinity of protein binding by factor 2 compared with standard non-damaged DNA [12]. Such profound reduction of complex instability can be addressed to significant changes in structural characteristics affecting dynamic properties of oxidized CTT [13]. Besides, observed alterations of electrostatic properties imposed by oxidation is an important factor contributing to TRF binding. In our previous works [13, 14] there were discussed some important consequences of telomere repeat unit oxidation. The application of MD/QM quenching method revealed significant stiffness of CTT as a result of CTT oxidation. This was related to skewness decrease of *roll* and *shift* distributions, increase of skewness and kurtosis of *opening* distributions and increase of kurtosis of *roll* distributions characterizing oxidized CTT with respect to canonical one. These structural changes imposed the increase of intermolecular interaction energies (IIE) characterizing stacking interactions of 8-oxoguanine with neighboring guanine molecules and hydrogen bonding of 8-oxoguanine with cytosine. The aim of this paper is to analyze consequences of TRF1 binding to canonical and oxidized telomere B-DNA oligomers on structure and energetics of telomere repeat unit. Although there were published important studies on dynamic and structural properties of oxidized B-DNA to our best knowledge consequences of TRF1 complexation and/or oxidation were not described so far. For example nowadays Naômé et al. [15] characterized hydration and ion binding patterns around double-stranded B-DNA containing 8-oxoguanine supporting existence of early recognition modes utilized by hOGG1 enzyme. Molecular dynamics simulation of clustered DNA damage sites that contain 8-oxoguanine were studied by Fuhimoto et al. [16]. Dodson and Lloyd [17] studied mechanism of substrate recognition for BER glycosylases *via* base flipping of DNA sequences containing 8-oxoguanine. The generated trajectories were used for identification of such properties of oligonucleotides in the vicinity of the altered site that are responsible for recognition. Dynamic behavior of DNA oligomers containing 8-oxoguanine was also studied by Cheng et al. [18]. Besides, short 1 ns molecular dynamics simulations were performed for elucidation of the effect of guanine lesion presence in B-DNA [19]. Much larger MD simulation were carried out by Fujimoto et al. combined with biomolecular visualization software [20]. However, most of the theoretical studies on 8-oxoguanine in B-DNA are related to explanation [21, 22] f activities of human oxoguanine glycosylase (hOGG1) [23–26] and TRF1 binding was analyzed with much lower intensity [27–30]. This paper concentrates on energetic stabilities of CTT characterized on post-SCF quantum chemistry level including not only BSSE corrections [31, 32] and necessary electron correlation contributions [33–35] but also many-body terms [35] for all analyzed systems. The methodology applied here was successfully tested in our previous investigations [36–39] for polymorphism-related heterogeneities of guanine stacking in B- and A-DNA forms [37], characteristics of *inter*- and *intra*-strand stacking interactions in d(CpG) and d(GpC) steps found in B-DNA, A-DNA and Z-DNA crystals [38], description of energetic heterogeneities in canonical and oxidized central guanine triad of B-DNA telomeric fragments [13, 14] and quantification of all possible *intra*-strand stacking interactions between nucleobases [39]. The essential feature of the approach applied here is characteristics of statistically significant probe of conformations and consequently obtaining of intermolecular interaction energies (IIE) distributions coming from quite long (40 ns) molecular dynamics sampling of analyzed oligomers. The averaged IIE values characterizing intermolecular interactions within CTT can then be supplied with corresponding standard deviations giving an impression of magnitude of structural and energetic fluctuations.

Methods

The meaningful conformations of any molecular system require adequate sampling over configurational hyperspace using one of many available theoretical approaches [40–44]. Among them molecular dynamics (MD) is widely accepted as an accurate tool for probing dynamics of many models of diverse biological systems within picoseconds or even microseconds time scales [41–44]. Along with an increase of computer power, time of simulations also continues to increase providing large amounts of data. This ensures that sampling will provide adequate insight into the dynamics of interactions. However, this is accomplished with interpretation problems since selection of the most representative structures (MRS) used for characteristics of the analyzed system is not a trivial task. One commonly applied approach of extraction of such a representative probe is clustering of molecular configurations according to their structural and energetic similarities. Unfortunately, there is no one ideal data-mining technique [45] providing univocal way of MRS selection and different algorithms lead to different descriptions [45–48]. As it was demon-

strated by Shao et al. [45] some algorithms tend to produce homogeneously sized clusters, whereas others have a tendency to produce singleton clusters. For these reasons in this paper we adopted another strategy for selection of MRS characterizing structural and energetic heterogeneities of canonical and oxidized B-DNA CTT present in free oligonucleotides and complexed with TRF1 protein in water solution. The central telomeric triad comprising d($G_2pZ_3pG_4$) sequence seems to be crucial from the perspective of TRF1 binding and this fragment was analyzed in details. Since conformations of dinucleotide steps are univocally characterized by a set of six values of helical parameters [49, 50] the distributions of these quantities instead of actual atomic coordinates were used for MRS selection. Using trajectories generated during 40 ns sampling with 1 ps step there were extracted *shift*, *slide*, *rise*, *roll*, *tilt* and *twist* values using X3DNA package [51]. Then after normalization of all distributions there were prepared histograms by division of the whole span into six equal intervals. Based on derived histograms the weighting coefficients were obtained for each base pair step parameter. Then there were randomly selected structures in number corresponding to estimated weights for each interval. This led to 36 structures for each probing distribution of each analyzed dinucleotide step. Typically this procedure was repeated ten times for generation of distinct probing distribution sets. The intermolecular interaction energies (IIE) were estimated using Amber forcefield [52, 53] for all dinucleotide step belonging to each probing distributions. For this purpose from selected pdb files corresponding to each MD trajectory snapshot there were cut dinucleotide steps for which sugar phosphate backbones was replaced with hydrogen atoms. Position of N-glycosidic hydrogen atoms were optimized according to geometric criterions. Obtained values of dinucleotide stabilization energies were used for histograms plotting. There were also prepared histograms corresponding to all analyzed structures for given dinucleotide step (360 values). This lead to a series of histograms of different shapes. For actual quantum chemistry computations the most representative set was selected by comparison to averaged histogram. The RMSD of histograms points were computed and the smallest value indicated the most representative set of conformations (MRS). The whole procedure was automatized by program written by authors. Initially different length of intervals in histograms, different number of selected structures for each interval and different number of probing sets were considered but the resulting IIE distributions were hardly dependent on these parameters. More details please find in supplementary materials (Fig. S1 and footnote). Only most representative sets of structures were used for precise intermolecular interaction energies (IIE) estimation at DF-MP2/aug-cc-pvDZ (aDZ) level of theory using MolPro package [54]. Since dinucleotide steps comprising stacked guanine molecules can exhibit significant non-negligible many-body contributions [35, 36] all IIE values were corrected using linear relationships proposed elsewhere [55]. In all cases where quantum chemistry calculations were applied the simplified model was used in which sugar-phosphate backbones were replaced with hydrogen atoms. However, the conformations of nucleobases exactly matching to ones occurring in MD runs were prepared according to procedure applied in our previous investigations [13, 14, 36–39]. All IIE values were also corrected for BSSE error according to the counterpoise scheme [31, 32].

As it was mentioned beforehand the subject of our interest is the telomere repeat unit (AGGGTT). The water solution structures of d(GpTpTpA$_1$p**G$_2$pG$_3$pG$_4$**pT$_5$pT$_6$pG$_3$**pG$_4$**pT$_5$pT$_6$pApGpGpG) oligomer in B-DNA form complexed with human TRF1 are available in NDB database [50] denoted as 1IV6 [56]. It comprises 20 distinct conformation of this protein-DNA tandem. These conformations were used as the source of initial structures of four studied systems (S1, S2, S3 and S4). Symbol S1 stands for free non-modified B-DNA oligomer, S2 represents oxidized analogue d(GpTpTpA$_1$p**G$_2$pZ$_3$pG$_4$**pT$_5$pT$_6$pApGpGpG), S3 denotes non-oxidized telomere oligomer in complex with TRF1 and S4 refers to oxidized telomeric fragment bound to TRF1. Symbol Z stands for guanine (in S1 or S3) or 8-oxoguanine (in S2 or S4). Central telomeric triad was marked using bold style. The available 20 conformations coming from NMR experiment were then the source of all S3 initial conformations. Preliminary structures of S1 were prepared by removing all atoms belonging to protein from each S3 conformation. Then S2 and S4 were build by replacement of G_3 with 8-oxoguanine in S1 and S3 respectively. Independent 2.5 ns molecular dynamics runs were performed for all 20 available conformations. Last 2 ns of all trajectory were used as the source of structural parameters collected every 1 ps. The time autocorrelation functions [57, 58] were plotted for ensuring that such short trajectories can still provide an adequate sampling of B-DNA dynamical structure. Since relaxation times of helicoidal parameters are proven to be shorter then 0.5 ns [58] their distributions appear to be well stabilized within applied time scale. Additionally different starting points ensure proper sampling of dynamic features of analyzed systems. The X3DNA package [51] was used for analysis of B-DNA conformation. Thus, trajectories corresponding to 40 ns dynamics for each studied oligomer (S1–S4) were obtained. Each oligomer was immersed in TIP3P water box and neutralized by 26 sodium cations. The periodic boundary conditions were imposed. All molecular dynamic simulations were done at room temperature with the aid of AMBER package [53] with Barcelona corrected forcefield [59].

Results and discussion

Trajectories generated during molecular dynamics simulations allow for quantitative characteristics of structural diversities imposed by oxidation and/or TRF1 complexation of analyzed telomere repeat units. Besides, a statistically significant probe of conformations taken for quantum chemistry calculations offers unique insight into heterogeneity of intermolecular interaction imposed by these two important factors. Due to commonly known inaccuracies of any available force-field parameterizations the reliable energetic analysis cannot be achieved using MM level. This is especially important for stacking interactions for which attractions are granted from dispersion forces and inclusion of electron correlation is a must [32, 34]. To our best knowledge this is the first such comprehensive attempt to characterize structural and energetic changes imposed by protein-DNA complexation using quantum chemistry approach.

Structural diversities of telomere repeat unit

Description of oligonucleotide chain flexibility and its sensitivity to external factors poses some challenges in the way of presentation. In order not to be obscured by the details coming from time evolution of so many parameters, the analysis of the whole distributions was done in terms of three statistical measures. Obviously the meadian value is the first choice representing the averages of particular distribution. The comparison of medians supplemented with values of standard deviation can directly reveal structural consequences of a particular factor acting on the oligomer. Since not all distributions are of normal type one can find such distributions which are characterized by almost the same median values (along with similar standard deviations) and still differences between them can be statistically significant. In such cases two additional statistical measures, namely skewness and kurtosis, are very useful since departures from normality are displayed by combinations of their values. The first quantity (skewness) simply evaluates the population asymmetry. Positive values of skewness indicate that the right part of distribution is more extended than the left one. Consequently existence of left tail on distribution plots is indicated by negative values of this parameter. Thus, the non-zero values of skewness reveal changes in preferences of particular conformations adopted by analyzed oligomers. The second quantity used here is kurtosis, which offers a very convenient way for characterizing the shape of distributions in sense of the degree of peakedness. In the case of normal distribution kurtosis is equal to zero and represents so-called mesokurtic distribution. A pure leptokurtic distribution has a higher peak than the normal distribution and has heavier tails. On the contrary a platykurtic distribution has a lower peak than a normal distribution and lighter tails. There is simple and direct structural interpretation of deviation from mezokurtic distributions, namely leptokurtic character indicates stiffness of analyzed oligomer structure with respect to a particular parameter. On the other hand flexibility with respect to a particular parameter is correlated with platykurticity and negative values of kurtosis. The distributions of all base step and base pair parameters characterizing flexibility of the whole telomeric repeat unit $d(A_1pG_2pZ_3pG_4pT_5pT_6)$ were analyzed. Each of dinucleotide steps is to be characterized by 18 parameters distributions for each of the analyzed chains. In supplementary materials detailed characteristics of obtained distributions are collected in Tables S1 and S2 along with graphical presentation (Fig. S2 and S3) of median values variations for all telomeric repeat units belonging to four analyzed oligomers. Additionally in Fig. 1 there are provided the most representative plots.

Although there are observed some alterations of median values, the majority of base pair distributions differ by less than standard deviations. This suggests that only modest changes are enforced on such base pair parameters as *shear*, *stretch*, *stagger, propeller* and *opening* by either of the analyzed factors (see Table S1, S2 and Fig. S1, S2). The only exceptions are visible for *buckle*. In Fig. 1 it is demonstrated that G_4 guanine (third one in CTT) is characterized by higher values of *buckle* in the case of S4 oligomer. Also T_5 and T_6 pairs are affected on the same way by TRF1 binding to both canonical and oxidized telomere fragments. Values of *buckle* represent bending of hydrogen bonded pairs along shorter molecular axis (perpendicular to DNA chain in major-minor groove direction). Besides, the median value of *propeller* describing mutual rotation of molecular planes around shorter molecular axis is lower for bases inside CTT of S1 and S2 systems. However, the difference between non-complexed and complexed dinucleotide chains is of order of standard deviations. This suggest that rotation of H-bonded bases in pairs constituting CTT is restricted in some extent after TRF binding. Reduction of this parameter suggest better coplanarity of nucleobases belonging to opposite chains and is the highest in the case of S3. Interestingly, kurtosis and skewness are rather small and almost identical for all distributions of all base pair parameters except of *stretch* and *opening*. In both cases skewness exceeds unity only for T_5 suggesting that there are a significant portion of structures adopting higher values than average of this parameter. The higher values of *stretch* the longer distance between hydrogen bonded pairs, while higher values of *opening* indicate asymmetrical trends of hydrogen bond breathing. Very high values of kurtosis were noticed in the case of Z_3 *opening* for S2 system and T_5 *stretching* for S3

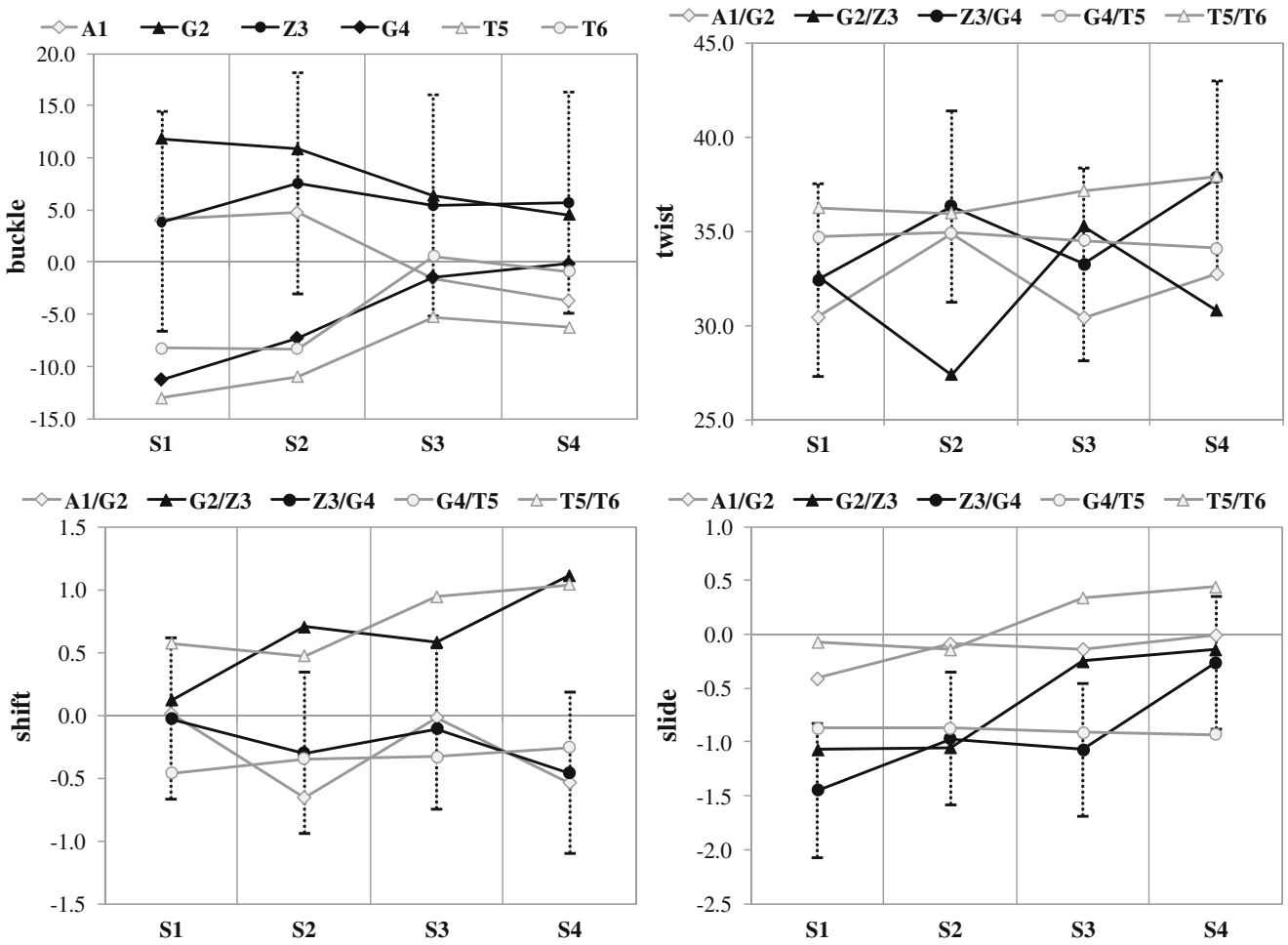

Fig. 1 Mean values of selected parameters defining conformations of nucleobases in telomere repeat unit

and S4 oligomers. Thus, oxidized guanine in CTT is the source of high stiffness if compared to non-modified oligomer. On the other hand binding of TRF1 to both oxidized and non-oxidized chains reduces this kind of rigidity to the degree typical for free non-altered oligomer. Furthermore, TRF1 complex formation imposes strong stiffness of T_5 *stretching* in S3 and S4 systems. Thus, these few mentioned alterations imposed on base pair parameters are the main structural consequences of oxidation or/and TFR1 binding in analyzed systems. In addition some interesting alterations are induced also on distributions of base pair parameters. In Fig. 1 there are presented three such spectacular instances. For example *shift* and *slide* are quite sensitive parameters affected by interactions of oxidized oligomer with analyzed protein. The median values of *shifting* of two base pairs along shorter molecular axis are reduced for Z_3/G_4 and increased for G_2/Z_3 pairs in S4 oligomer. This is accomplished by the significant reduction of skewness of *shift* populations of G_2/Z_3. This suggests that S4 system exhibits strong tendency toward reducing *shift* values to ones typical for S1 oligomer. Also increased *sliding* of Z_3/G_4 and G_2/Z_3 pairs found for S4 system suggests significant movement along longer molecular axis of these two pairs imposed by TRF1. Furthermore, significant reduction of base pairs *twisting* is observed for S2 and S4 oligonucleotides indicating much smaller rotation of base pairs within $d(G_2/pZ_3)$ dinucleotide steps. Also, interactions with protein change also *roll* values characterizing S4 structure. *Rolling* of base step pairs describes mutual rotation of base pairs around shorter molecular axis. Negative *roll* values of Z_3/G_4 indicate increasing distance between stacked base pairs from major grove side. These changes are also accomplished with changes in *tilt* values describing Z_3/G_4 base pair of S4 structures suggesting tendency of increasing of distance between stacked bases on right side of major grove. Besides, there is observed significant *twisting* of Z_3/G_4 base step pair of S3 and S4 that is much larger if compared with S2 and S3 oligomers. Above statements confirm that binding of TRF1 to canonical or oxidized telomere repeat unit is an important factor contributing to structure and dynamics of analyzed oligomers. The most important alterations im-

posed on geometry of CTT's that were discussed above are summarized in Fig. 2. Length of vectors and directions of angles schematically represents magnitude of differences.

Purines rings overlapping

In the central telomeric triad (CTT) three purine rings can overlap forming two pairs of *intra*-strand stacking. It is reasonable to expect that any changes imposed on structure and dynamics of CTT can lead to alterations of base-over-base displacement. This feature can be expressed qualitative by the analysis of fluctuations of overlapping area (in $Å^2$) between polygons defined by atoms on successive bases within the same strand. Polygons are projected on the mean plane of the analyzed base-pair step. Such values are the measure of base ring overlaying excluding exocyclic atoms. Observed fluctuations of overlapping areas for two successive purines belonging to the first strand were plotted in Fig. 3 for all analyzed oligomers. Very interesting observation can be made from both presented plots and provided medians. First of all, native B-DNA telomere is a very flexible structure and overlapping area of the first two guanine molecules in CTT changes in wide range (from 0 to $6 Å^2$). Supplied median values as well as histogram plots in Fig. 3 support a quite flexible nature of GGG triad in native telomere repeat. The comparable values of medians and standard deviations of G_2/G_3 and G_3/G_4 suggest symmetrical movements of both G-C pairs. Replacement of G_3 with 8-oxogunaine has profound consequence on the area of overlapping. Momentous increase of $G_2/8oxoG_3$ stacking contacts and slight decrease of $5'\text{-}Z_3/G_4\text{-}3'$ overlaying is observed in the case of S2 system. Hence, symmetrical GGG triad become much more asymmetrical after oxidation of central guanine. Interestingly, similar consequences on overlapping areas are observed as a result of TRF1 binding to S1 structure. In the case of S3 oligomer the contacts of G_2/G_3 pair are significantly increased with unchanged G_3/G_4 overlapping. Oxidation of guanine in CTT in S4 complex even enhance this effect. Additionally reduction of overlapping areas in $d(Z_3pG_4)$ dinucleotide steps is to be noticed. One can expect that the *intra*- strand interactions should be significantly affected by such changes of CTT structure. This aspect will be discussed in the next section. Thus, both oxidation and TRF1 binding can have significant influence on the overlapping of aromatic rings in central telomeric guanine triad.

Energetic consequence of oxidation and TRF1 binding

Structural alterations imposed by oxidation and complexation with TRF1 must affect intermolecular interactions between bases constituting central telomeric triad. Three distinct types of contacts determine IIE within central telomeric triad, namely hydrogen bonding, *intra*- and *inter*-strands stacking. They are systematically studied below for population comprising most representative structures extracted according to procures described above. As it was previously demonstrated [34–36] interactions in d(GpG) dinucleotide steps can exhibit significant non-additive character reaching several kcal mol^{-1}. Furthermore, many-body contributions to stabilization of dinucleotide steps comprising 8-oxoguanine are also non-negligible [55]. Fortunately, sum of all many

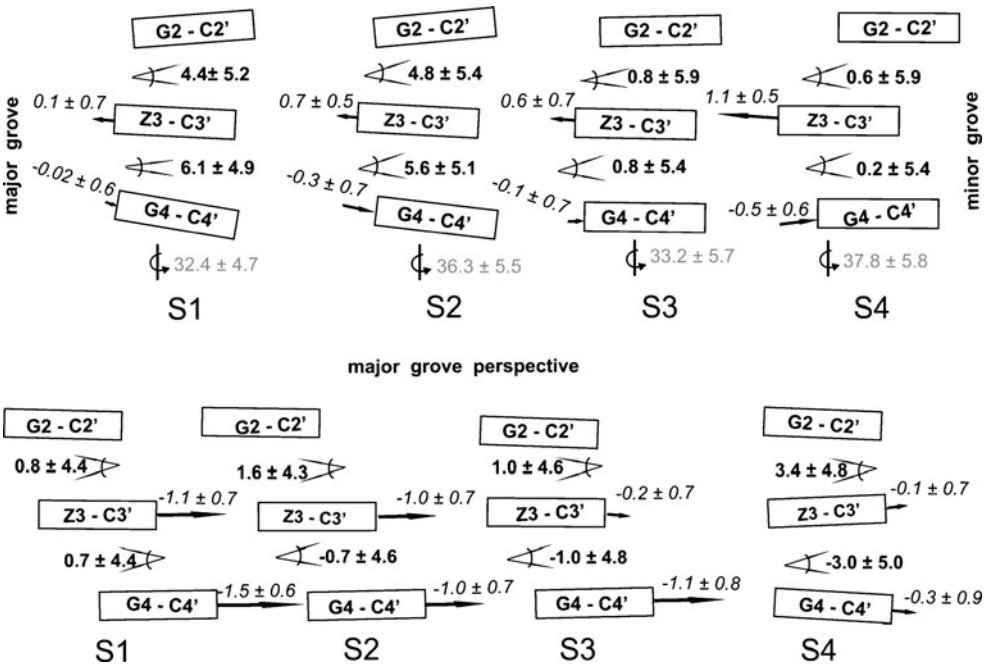

Fig. 2 Schematic representation of mean values and corresponding standard deviations of parameters that are strongly affected by oxidation and/or complexation by TRT1 protein. In upper view normal style was used for representing values of *shift* (Å), in italics there are provided *roll* (°) values and numbers in gray represent *twist* (°) values. In the lower view *slide* (Å) and *tilt* (°) are presented in normal and bold style, respectively

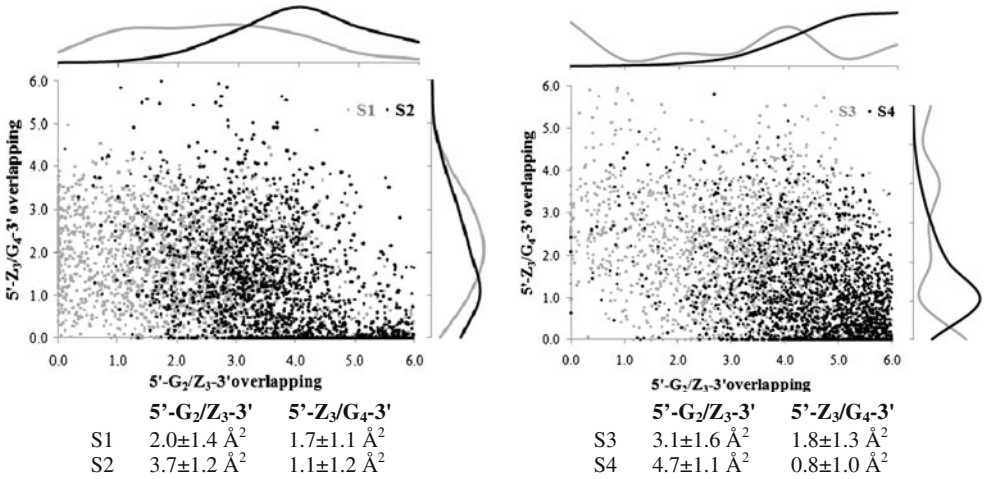

	5'-G_2/Z_3-3'	5'-Z_3/G_4-3'
S1	2.0±1.4 Å^2	1.7±1.1 Å^2
S2	3.7±1.2 Å^2	1.1±1.2 Å^2

	5'-G_2/Z_3-3'	5'-Z_3/G_4-3'
S3	3.1±1.6 Å^2	1.8±1.3 Å^2
S4	4.7±1.1 Å^2	0.8±1.0 Å^2

Fig. 3 The distributions of the overlapping area (in Å^2) between polygons defined by base ring atoms on successive bases excluding areas of exocyclic atoms. Median values along with standard deviations are provided for both stacked pairs in central telomeric triad of analyzed oligomers. Symbol Z represent guanine (for S1 and S3) or 8-oxoguanine (in case of S2 and S4). Points correspond to every 10 ps snapshots. Histogram plots for all distributions were supplied in edges of corresponding axis

body terms scale linearly with non-additive part and simple correction is possible. Regression analysis presented in Fig. 4 demonstrate that many-body contributions are not very high and in average are equal to −1.8 kcal mol^{-1} for non-oxidized dinucleotide steps and −2.4 and −2.8 kcal mol^{-1} for d(GpZ) and d(ZpG), respectively. Since many body contributions can change depending of nucleobases conformations, all additive IIE values were corrected according to regression formula presented in Fig. 4.

Base-base interactions in CTT

Results of IIE calculations were presented in Fig. 5 and Table 1. In the case of purine/purine *intra*-strand stacking

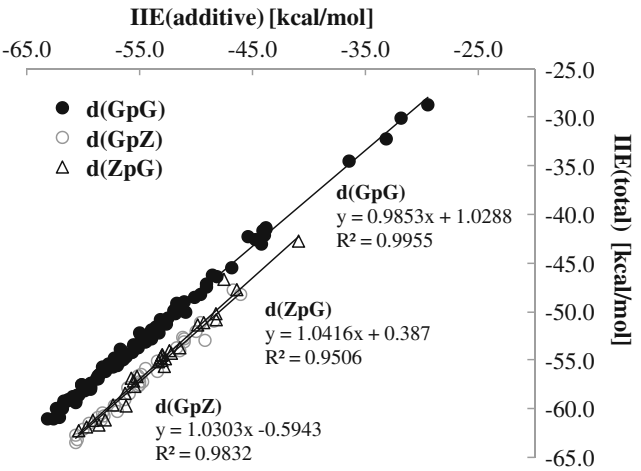

Fig. 4 Regression analysis between intermolecular interactions in dinucleotide steps estimated using pair-wise additivity (IIE(additive)) and full inclusion of all many body contributions (IIE(total)) [55]

width of IIE distribution is about 2 kcal mol^{-1} in terms of half of the most often occurring IIE values (differences between bottom and top 25% of values). In the case of G_2/G_3 in S1 oligomers the range of observed *intra*-stacking starts from −5.6 and −0.7 kcal mol^{-1}. The *inter*-strand stacking of complementary cytosine molecules ranges between −6.1 and +1.3 kcal mol^{-1}. This gives an impression of the influence of structural fluctuations generated during MD run on the heterogeneities of actual values of intermolecular interactions. Due to non-normal distributions of intermolecular interaction energies instead of mean or median values the most frequently occurring energies (IIE^{MFO}) are used as the main energetic characteristics of intermolecular interactions. It simply corresponds to localization of maximum on smoothed histograms. Plots characterizing distributions of *intra*-strand stacking of two purines or two pyrimidines are exemplified in Fig. 5. From these data interesting trends can be concluded. First of all *intra*-strand stacking involving 8-oxoguanine in G_2/Z_3 pairs (of S2 and S4) is in average 3.5 kcal mol^{-1} stronger than in G_2/G_3 pairs (of S1 and S3). This significant increase of stacking of oxidized guanine is the main consequence of observed structural differences between modified and non modified chains of telomere repeat unit. Interestingly, irrespectively of the presence or absence of TRF1 protein the *intra*-strand stacking of 8-oxoguanine with guanine is significant context-dependence since IIE^{MFO} of G_2/Z_3 and Z_3/G_4 sequences differ by more than values of standard deviations. Purines involved in the former pair interact much stronger than the latter. This rationale explains the observed discrepancies in overlapping areas. The *intra*-strand stacking of C_2/C_3 cytosine molecules are sensitive to TRF1 interactions with oxidized telomere repeat unit. Statistically significant decrease of IIE^{MFO} by about

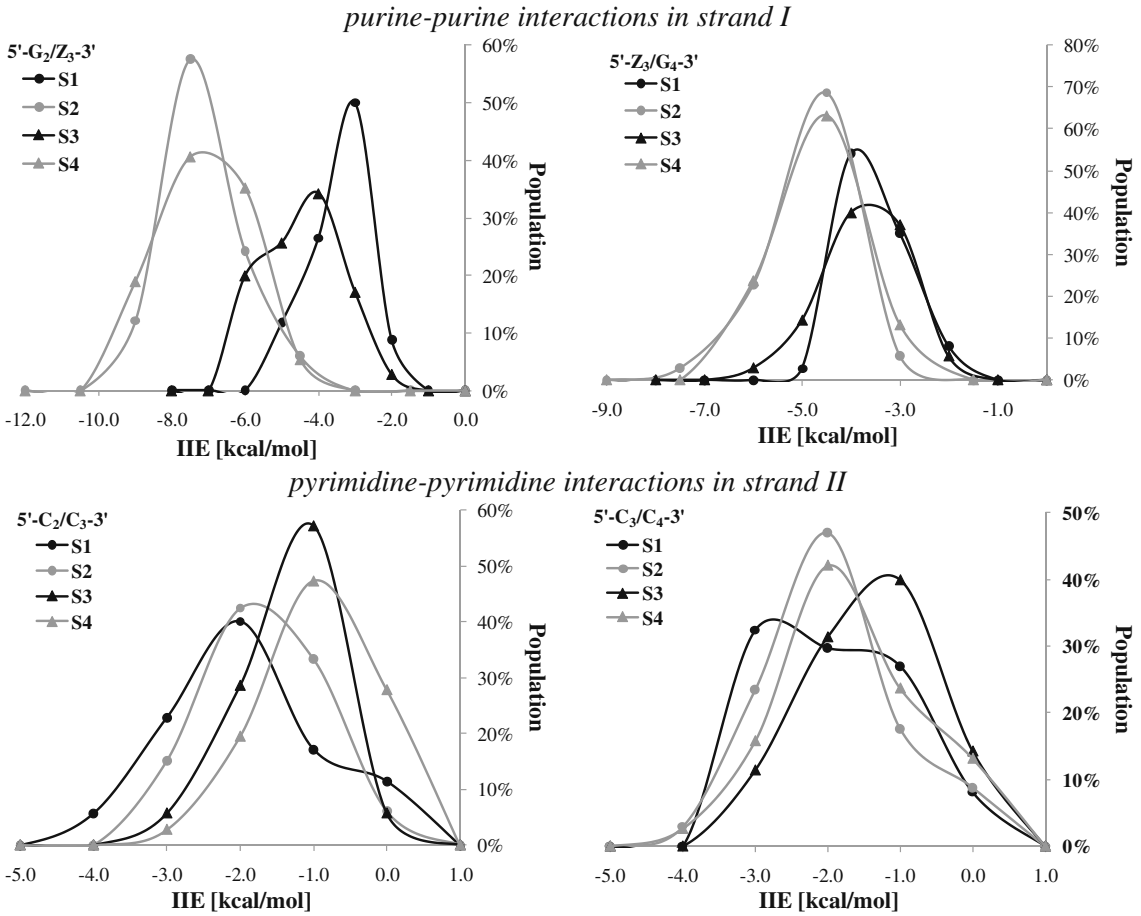

Fig. 5 Distributions of *intra*-strand stacking interactions in CTT of analyzed oligomers. In legends there are provided probabilities that the difference in the median values between the two groups (S3 with respect to S1 and S4 against S2) is statistically significant. In the case of $P<0.001$ the possibility that the difference is merely due to random sampling variability is excluded

2 kcal mol^{-1} is noticed in the case of C_2/C_3 stacking. For the rest of *intra*-strand stacking pairs of two cytosine molecules there is no observed significant influence of guanine oxidation and TRF1 binding. Besides, *inter*-strand stacking occurring in CTT is sequence dependent. For example 5′-Z_3|C_4-5′ (in d(ZpG)) is about 30% weaker than 3′-Z_3|C_2-3′ (in d(GpZ)) in all oligomers except S4. In this case both these *inter*-strand interactions are almost identical.

Table 1 Values of the most frequently occurring intermolecular interactions IIE^{MFO}[kcal mol^{-1}] in central d($G_2pZ_3pG_4$) fragment of telomere repeat unit, where Z stands for G or 8oxoG. The values of standard deviation were estimated for populations comprising 100 snapshots. Symbol S1 represents canonical double strand, S2 designates oxidized one, S3 indicates canonical strand with bounded TRF1 and S4 denotes oxidized B-DNA in complex with TRF1

[a] Corrected according to linear regressions presented in Fig. 4

		S1	S2	S3	S4
d(GpZ)	G_2/Z_3	−3.1±1.0	−7.4±1.1	−4.2±1.3	−7.0±1.3
	C_2/C_3	−2.1±1.2	−1.8±1.3	−1.1±0.8	−0.9±1.2
	5′-G_2|C_3-5′	−2.2±1.2	−2.0±1.3	−2.3±1.4	−2.3±1.0
	3′-Z_3|C_2-3′	−3.0±1.6	−3.1±0.9	−2.8±0.7	−3.3±2.4
	5′-G_2–C_2-3′	−21.3±2.2	−20.4±2.2	−20.6±2.5	−21.5±2.4
	3′-Z_3–C_3-3′	−21.3±1.6	−20.7±2.1	−21.6±2.7	−21.2±3.2
	dinucleotide[a]	−50.5±2.8	−59.5±3.7	−53.0±3.5	−58.9±3.5
d(ZpG)	Z_3/G_4	−3.8±0.6	−4.6±0.9	−3.6±0.9	−4.6±1.0
	C_3/C_4	−2.6±1.0	−2.1±1.1	−1.3±0.9	−1.9±1.0
	5′-Z_3|C_4-5′	−2.0±1.0	−2.2±0.8	−2.5±1.2	−2.3±0.9
	3′-G_4|C_3-3′	−2.9±1.4	−2.3±2.0	−2.1±1.2	−2.1±1.0
	3′-G_4–C_4-3′	−21.0±2.1	−21.6±2.2	−21.0±2.5	−20.0±2.6
	dinucleotide	−52.7±2.8	−58.1±4.3	−50.7±3.1	−56.0±3.5

Presence of the oxidized guanine also influences *inter*-strand stacking of guanine with cytosine making 3′-G_4|C_3-3′ interactions about 1.4 kcal mol^{-1} stronger than for 5′-G_2|C_3-5′ in S2. No differences in strength of stronger hydrogen bonds are observed for all canonical and oxidize Z-C pairs. It is also interesting to know if any compensation effects take place of previously discussed changes in base–base interactions for higher ordered structures. Thus, dinucleotide steps were considered. The corresponding IIE values were estimated assuming pair-wise additivity supplemented with linear correlation corrections for many-body contributions (see Fig. 4). The most straightforward conclusion drawn from data collected in Table 1 is that the overall stabilization energy of all oxidized dinucleotide steps are significantly higher compared to canonical ones. The gain in IIE^{MFO} interaction energies is about 9 kcal mol^{-1} and significantly exceeds values of standard deviations. These changes were proven to be statistically significant. Thus, for dinucleotide steps oxidation has profound stabilization effect for all pairs in CTT originating from increase of *inter*- and *intra*-strand stacking of 8-oxoguanine. On the other hand interaction with TRF1 does not change significantly stabilities of dinucleotide steps constituting central telomeric triad.

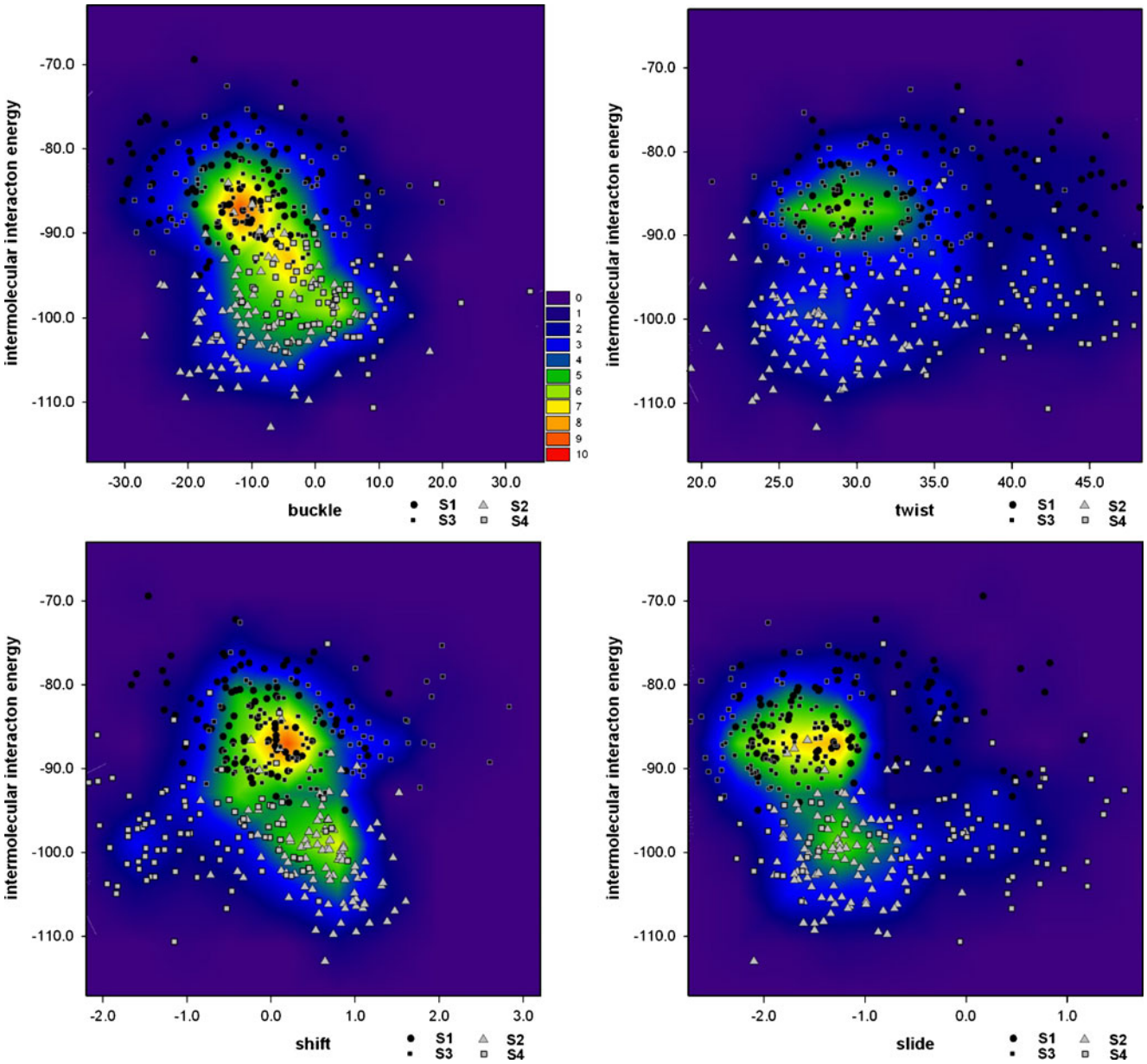

Fig. 6 Distributions of the sum of intermolecular interactions energies in d(GpZpG) central telomeric triad as a function of values of selected parameters for all analyzed systems. The color spectrum representing the total percentage of populations obtained from two-dimensional histograms has the same scale for all contour maps

Structure to energy relationships

In previous sections there were discussed significant structural and energetic alterations as a consequence of oxidation and/or TRF1 protein binding to telomeric repeat unit. It is interesting to see if there are any direct structure to energy relationships not only on the level of base–base interactions but on a bigger scale. Those parameters, which distributions were non-changed by two analyzed factors were excluded from the analysis, while for those distributions, which were proven to be statistically significant two dimensional contour maps were prepared. In Fig. 6 there are presented scattering plots characterizing actual correlation between the stabilization energy in the whole tetramer that forms central telomeric triad d(GpZpG) and values of *buckle*, *twist*, *shift*, and *slide*. These distributions were over imposed on the contour map representing percentage of particular structure with given IIE value. For this reason the whole spectrum of values was divided into ten equal intervals and two-dimensional histograms were estimated and presented as smoothed contour maps. From such graphs it is clearly visible almost perfect energetical separation of $d(G_2pG_3pG_4)$ and $d(G_2pZ_3pG_4)$ trinucleotides. Besides, structural heterogeneities can also be seen. For example *buckle* can adopt values from interval (−36°, +36°). The range of most frequently occurring buckle values is quite similar for canonical and oxidized trinucleotides, but there are structures characterized occasionally by values outside of this region. It is also visible that *buckle* distributions of S4 system are significantly shifted toward higher values with respect to other oligomers. This is in good accord with conclusions drawn from Fig. 1. *Twist* distributions presented in Fig. 6 posses different properties. The most probable structures found in the range between 25° and 35° come from non-oxidized systems (S1 and S3). On the contrary much higher flexibilities with respect to *twist* values are observed for S2 and S4. Also the fluctuations of *shift* and *slide* can be momentous for all analyzed structures and cover a range of more than 4 Å for both of these step parameters. Interestingly, the discrepancies between *shift* distributions of S3 and S4 are well documented in Figs. 6 and 7. Much higher stiffness of this parameter is to be related to S1 and S3 structures. Similar conclusion can be drawn from slide distributions. In this case however, significantly lower values are observed for S3. Finally there is a spectacular consequence of TRF1 binding to oxidized telomere repeat unit. Significant population of CTT structures found in S4 adopts positive values of *slide* and negative values of *shift*. This is observed only in the case of S4. The rest of the populations are characterized by negative values of *slide* (<−1.0 Å) and smaller than 1 Å absolute values of *shift*. This is most direct consequence of TRF1 binding to oxidized telomere repeat unit, which distinguishes univocally such complex from canonical ones.

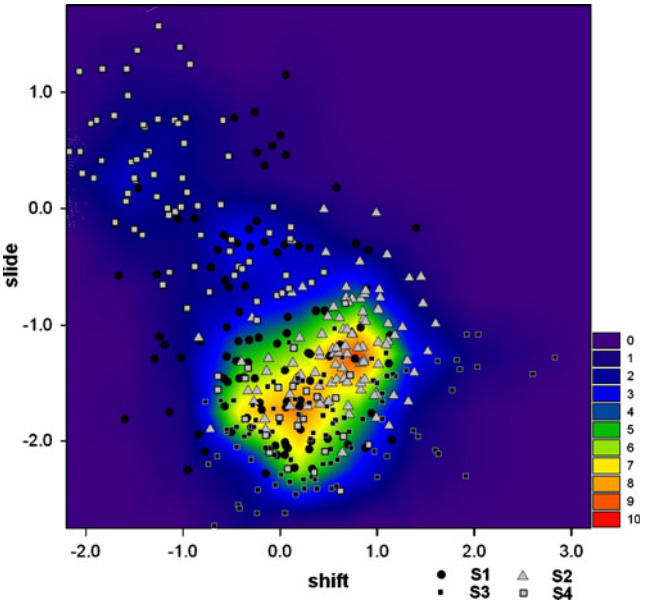

Fig. 7 Correlations between *shift* and *slide* values characterizing Z_3/G_4 step for all analyzed oligonucleotide systems. Notation is the same as in Fig. 6

Conclusions

The B-DNA of $d(A_1pG_2pG_3pG_4pT_5pT_6)$ sequence constituting telomeric repeat unit is significantly affected by both oxidation and binding of TRF1 protein. Presented data clearly identified structural and energetic consequences imposed on central telomeric triad by these two factor. The occurrence of 8-oxoguanine in CTT is the source of high stiffness if compared to non-modified oligomer. The origin of this property comes from significant alteration of intermolecular interactions of 8-oxoguanie. Presence of this lesion in CTT leads to an important increase of *intra*-strand stacking involving 8-oxoguanine in G_2/Z_3 pair by about 3.5 kcal mol^{-1} if compared to G_2/G_3 pair. Also oxidized guanine influenced *inter*-strand stacking of guanine with cytosine making $3'\text{-}G_4|C_3\text{-}3'$ interactions about 1.4 kcal mol^{-1} stronger than for $5'\text{-}G_2|C_3\text{-}5'$ in oxidizes oligonucleotides. The sequence dependent *inter*- and *intra* stacking involving 8-oxoguanine are observed. In the case of 8-oxoguanine present in d(ZpG) sequence significantly reduces of base–base interactions if compared with d(GpZ) dinucleotide steps. The increased stability observed for base–base interactions has cumulative character and is typical also for di- and tri-nucleotides. Although for some conformations there are observed non-negligible contributions coming from many-body terms still dinucleotides and the whole CTT are significantly more stable with respect

to their canonical equivalents. The observed changes in the intermolecular interactions originate from structural alterations imposed by TRF1 binding to canonical and oxidized telomere B-DNA. The first and most direct consequence of TRF1 binding to oxidized telomere repeat unit is alteration of *shift-slide* correlations. Only in the case of TRF1 complex formed with oxidized CTT significant population adopts positive values of *slide* and negative values of *shift*. This in turn leads to large differences in purine-purine overlapping in oxidized structures. Thus, oxidized structures of telomere repeat unit are more sensitive to interactions with protein ligands especially for Z_3/G_4 stacked pairs.

References

1. Fairall L, Chapman L, Moss H, de Lange T, Rhodes D (2001) Mol Cell 8:351–361
2. Lundblad V (2000) Mutat Res 451:227–240
3. Chong L, van Steensel B, Broccoli D, Erdjument-Bromage H, Hanish J, Tempst P, de Lange T (1995) Science 270:1663–1667
4. Harley CB, Futcher AB, Greider CW (1990) Nature 345:458–460
5. von Zglinicki T, Serra V, Lorenz M, Saretzki G, Lenzen-Grossimlighaus R, Gressner R, Risch Steinhagen-Thiessen E (2000) Lab Invest 80:1739–1747
6. Bodnar AG, Ouellette M, Frolkis M, Holt SE, Chiu CP, Morin GB, Harley CB, Shay JW, Lichtsteiner S, Wright WE (1998) Science 279:349–352
7. Broccoli D, Smogorzewska A, Chong L, de Lange T (1997) Nat Genet 17:231–235
8. Court R, Chapman L, Fairall L, Rhodes D (2005) EMBO Rep 6:39–45
9. Hanaoka S, Nagadoi A, Nishimura Y (2005) Protein Sci 14:119–130
10. Tchirkov A, Lansdorp PM (2003) Hum Mol Genet 12:227–232
11. von Zglinicki T (2002) Trends Biochem Sci 27:339–344
12. Opresko PL, Fan J, Danzy S, David M, Wilson DM III, Bohr VA (2005) Nucleic Acids Res 33:1230–1239
13. Cysewski P, Czeleń P (2009) J Mol Model 15:607–613
14. Cysewski P, Czeleń P (2007) J Mol Model 13:739–750
15. Naômé A, Schyman P, Laaksonen A, Vercauteren DP (2010) J Phys Chem B 114:4789–4801
16. Fujimoto H, Pinak M, Nemoto T, O'neill P, Kume E, Saito K, Maekawa H (2005) J Comput Chem 26:788–798
17. Dodson ML, Lloyd RS (2001) Mutation Res 487:93–108
18. Cheng X, Kelso C, Hornak V, de los Santos C, Grollman AP, Simmerling C (2005) J Am Chem Soc 127:13906–13918
19. Ishida H (2002) J Biomol Struct Dyn 19:839–851
20. Fujimoto H, Pinak M, Nemoto T, Sakamoto K, Yamada K, Hoshi Y, Kume E (2004) J Mol Struct THEOCHEM 681:1–8
21. Bruner SD, Norman DP, Verdine GL (2000) Nature 403:859–866
22. Hanaoka S, Nagadoi A, Nishimura Y (2005) Protein Sci 14:119–130
23. Pinak M (2003) Comput Chem 24:898–907
24. Pinak M (2003) Comput Biol Chem 27:431–441
25. Pinak M (2002) J Mol Struct THEOCHEM 583:189–197
26. Miller JH, Fan-Chiang CCP, Straatsma TP, Kennedy MA (2003) J Am Chem Soc 125:6331–6336
27. Zhang RB, Xu H, Qu ZW, Zhang XK, Ai CX, Zhang QY (2002) J Mol Struct THEOCHEM 586:167–175
28. Tchirkov A, Lansdorp PM (2003) Hum Mol Genet 12:227–232
29. von Zglinicki T (2002) Trends Biochem Sci 27:339–344
30. Hanaoka S, Nagadoi A, Nishimura Y (2005) Protein Sci 14:119–130
31. Jansen HB, Ross P (1969) Chem Phys Lett 3:140–143
32. Boys SF, Bernardi F (1970) Mol Phys 19:553–566
33. Hobza P, Šponer J (1999) Chem Rev 99:3247–3276
34. Černý J, Hobza P (2005) Phys Chem Chem Phys 7:1624–1626
35. Hobza P, Sponer J (2002) J Am Chem Soc 124:11802–11808
36. Cysewski P (2010) Int J Quantum Chem. doi:10.1002/qua.22435
37. Cysewski P (2008) J Mol Struct THEOCHEM 865:36–43
38. Cysewski P (2009) J Mol Model 15:597–606
39. Cysewski P (2009) New J Chem 33:1909–1917
40. van Gunsteren WF, Berendsen HJC (1999) Angew Chem Int Ed Engl 29:992–1023
41. Hansson T, Oostenbrink C, van Gunsteren WF (2002) Curr Opin Struct Biol 12:190–196
42. Kollman PA, Massova I, Reyes C, Kuhn B, Huo S, Chong L, Lee M, Lee T, Duan Y, Wang W, Donini O, Cieplak P, Srinivasan J, Case DA, Cheatham TE III (2000) Acc Chem Res 33:889–897
43. Karplus M, McCammon J (2002) Acad Nat Struct Biol 9:646–652
44. Cheatham TE III, Kollman PA (2000) Annu Rev Phys Chem 51:435–471
45. Shao J, Tanner SW, Thompson N, Cheatham TE III (2007) J Chem Theory Comput 3:2312–2334
46. Lyman E, Zuckerman DM (2006) Biophys J 91:164–172
47. Feher M, Schmidt JM (2003) J Chem Inf Comput Sci 43:810–818
48. Gabarro-Arpa J, Revilla R (2000) Comput Chem 24:696–698
49. Diekmann S (1989) J Mol Biol 205:787–791
50. Berman HM, Olson WK, Beveridge DL, Westbrook J, Gelbin A, Demeny T, Hsieh SH, Srinivasan AR, Schneider B (1992) Biophys J 63:751–759
51. Lu XJ, Olson WK (2003) Nucleic Acids Res 31:5108–5121
52. Case DA, Cheatham TE III, Darden T, Gohlke H, Luo R, Merz KM, Onufriev A Jr, Simmerling C, Wang B, Woods R (2005) J Comput Chem 26:1668–1688
53. Case DA, Darden TA, Cheatham TE III, Simmerling CL, Wang J, Duke RE, Luo R, Merz KM, Wang B, Pearlman DA, Crowley M, Brozell S, Tsui V, Gohlke H, Mongan J, Hornak V, Cui G, Beroza P, Schafmeister C, Caldwell JW, Ross WS, Kollman PA (2004) AMBER 10. University of California, San Francisco
54. Werner HJ, Knowles PJ, Lindh R, Manby FR, Schutz M, Celani P, Korona T, Rauhut G, Amos RD, Bernhardsson A, Berning A, Cooper DL, Deegan MJO, Dobbyn AJ, Eckert F, Hampel C, Hetzer G, Lloyd AW, McNicholas SJ, Meyer W, Mura ME, Nicklaß A,Palmieri P, Pitzer R, Schumann U, Stoll H, Stone AJ, Tarroni R, Thorsteinsson T (2006) MOLPRO, a package of ab initio programs designed by Werner HJ and Knowles PJ, Version 2006.0 (Patch 2006.1). Cardiff UK
55. Cysewski P (2010) J Mol Model (JMMO1145—accepted for publication in this issue)
56. Nishikawa T, Okamura H, Nagadoi A, Konig P, Rhodes D, Nishimura Y (2001) Structure 9:1237–1251
57. Azbel MY (1995) Phys Rev Lett 75:168–171
58. Ponomarev SY, Thayer KM, Beveridge DL (2004) PNAS 101:14771–14775
59. Pérez A, Marchán I, Svozil D, Šponer J, Cheatham TE III, Laughton CA, Orozco M (2007) Biophys J 92:3817–3829